

Article

Agates from Western Atlas (Morocco)—Constraints from Mineralogical and Microtextural Characteristics

Jaroslav Pršek *, Magdalena Dumańska-Słowik , Tomasz Powolny, Lucyna Natkaniec-Nowak, Tomasz Toboła, Damian Zych and Dominika Skrepnicka

Faculty of Geology, Geophysics and Environmental Protection, AGH UST, University of Science and Technology, 30 Mickiewicz Av., 30-059 Krakow, Poland; dumanska@agh.edu.pl (M.D.-S.); powolny@agh.edu.pl (T.P.); natkan@agh.edu.pl (L.N.-N.); tob@geolog.geol.agh.edu.pl (T.T.); zychukr@gmail.com (D.Z.); skrepnicka@gmail.com (D.S.)

* Correspondence: prsek@yahoo.com

Received: 13 January 2020; Accepted: 19 February 2020; Published: 22 February 2020



Abstract: Agate samples collected from the vicinity of Asni and Agouim (Western Atlas, Morocco) were investigated using microscopic observations supported by Raman micro-spectroscopy. The agates are marked by the presence of various microtextures typical of epithermal vein deposits, including jigsaw-puzzle, feathery, and lattice-bladed. The first two indicate that the formation of agates was likely marked by recrystallization of metastable silica phases (i.e., opaline silica or massive chalcedony). The presence of lattice-bladed (after barite and calcite) quartz may be, in turn, ascribed to the boiling-related conditions that could have triggered the formation of abundant copper and iron sulfides found within silica matrix. Additionally, the local occurrence of growth lines (so-called Bambauer quartz) and intergrowth of length-slow and length-fast chalcedony are linked to the variations of physico-chemical conditions during rock formation (alkaline-acidic). According to Raman spectroscopy, silica matrix of the agates is made of α -quartz with a local admixture of moganite (from 0.0 up to 78 wt.%), but also contains numerous solid inclusions of hematite, celadonite, as well as poorly-organized carbonaceous material and rutile. These phases were likely emplaced during low-temperature hydrothermal activity of SiO_2 -bearing fluids that originated from post-magmatic hydrothermal activity developed within host rocks and/or meteoric waters.

Keywords: Moroccan agates; ore minerals; microtexture; moganite; Raman spectra

1. Introduction

Agates are defined as banded and colorful chalcedony with admixture of other silica polymorph varieties and paragenetic minerals [1–3]. They are mainly found within fine-grained volcanic rocks and their tuffs [4], but are also known from sedimentary and hydrothermal environments [2,3]. Overall, there are two main types of agates that can be distinguished based on the form of their occurrence: (1) lithophile type filling vugs created by vesiculation and (2) fissure type that occupy veins and cracks within the surrounding rocks. Other features of agates are strongly varied and exceptional (e.g., moss or botryoidal appearance). They show significant diversity in wealth of colors, structural and textural features, shape, and patterns, which make each specimen a unique product of inanimate nature both under micro and macroscale.

Despite the worldwide occurrences and numerous published papers, there are still some problems concerning agate nomenclature, classification, and formation, which are not completely solved. From a textural point of view, agate represents a banded chalcedony, which incorporates other SiO_2 polymorphs and varieties (e.g., [4–10]). Conversely, the mineralogical/petrographical approach assumes that agate can be considered as a rock that consists mainly of low-quartz, with admixture of other mineral phases

such as moganite, opal C, and coloring agents including hematite, goethite, calcite, barite, zeolite, and many others [4,11]. That agates could originate either from the direct precipitation of silica minerals from hydrothermal fluids or the deposition of an amorphous silica gel that subsequently crystallizes or matures by diagenetic processes is still a topic of controversy [11].

The first note about agate occurrences in the vicinity of the Medina oasis (Al Madinah) in Saudi Arabia was mentioned about 3000 BC [12]. Since then, new findings about agate deposits and smaller occurrences were systematically reported [12,13]. Currently, the largest agate deposits in the world are found in Uruguay and Brazil (Rio Grande do Sul province). Less significant occurrences are found in nearly each country of the world [14].

Agates from Morocco, discovered in the 1940s, are considered quite a novelty in the stone market over the few last decades [15–17]. They are found within Triassic basaltic rocks in many places in the High Atlas Mts. (e.g., near Sidi Rahal, Asni, Agouim-Al Hama, and Tizi-n-Tichka) as well as in the Middle Atlas Mts. (e.g., Kerrouchen and Ahouli region). Agate mineralization is pervasively accompanied by other products of hydrothermal activity in this area such as ore deposits of manganese, iron, copper, gold, and lead-zinc (e.g., [18–23]).

Moroccan agates have been systematically investigated by authors of this work for over 12 years. Up to now, reports on agates from Sidi Rahal and Kerrouchen are published [24,25]. In this contribution, the next two occurrences of agates in the Atlas Mts (i.e., Asni and Agouim), are investigated using microscopic methods supported by Raman micro-spectroscopy. The detailed microtextural description, along with the distribution of silica polymorphs and solid inclusions, were provided to put constraints on formation conditions of agates from this region and determine the possible sources of silica-bearing fluids. Moreover, the aim of this report is to highlight both the similarities and differences between agates from these four localities in Morocco to broaden the current knowledge of agate mineralization within the basaltic rocks of the Atlas Mts.

2. Geological Settings and Localizations of Agates Occurrences in Morocco

The Atlas Mountain range is located in the northern part of Africa. It has a length of more than 2000 km, from the Atlantic coast in Morocco up to Kabiska Bay on the coast of the Mediterranean Sea. The range is the continuation of the Alpine orogenic system. The Atlas unit was folded, deformed, dislocated, and upthrust at the beginning of Paleogene. Later on, it systematically changed during other tectonic activity up to the Pleistocene age [26]. As a result, two main dislocating and fold zones can be distinguished: the inner part with Middle, Upper, Sahara, and Antiatlas [27] and other part with Tellian Atlas and Rif Mountains [28]. These two zones are divided by Morocco Meset (200–1500 m above sea level (m. a.s.l.)) and Shott zone (750–1000 m. a.s.l.) and they comprise rocks of various mineral compositions and age.

The High Atlas is built of Paleozoic rocks, mainly quartzites, limestones, and volcanic rocks connected with the Hercynian orogenesis. The upper parts of the High Atlas Mts. are covered by thick series of folded and unfolded Jurassic and Cretaceous limestones as well as lower Paleogene series of limestone-sandstones. Agate occurrences are known from many localities in the High Atlas, as well as from the tectonic forelands of this unit (Figure 1). The richest deposits of agates are in Tizi-n-Tichka-Agouim-Al Hama, Sidi Rahal, and Asni regions, but some new deposits with similar characteristics are found in other parts of the volcanic suite of High Atlas [15].

Sidi Rahal is a small village about 15 km east of Ait Ourir, which became known from a quarry of basalts with agate mineralization. Triassic basaltoides have a thickness up to 3.0 km in that region [15]. This volcanic outcropping is half-moon shaped with a size of 110 × 70 km. Basaltoides frequently contain spherical or almond-shaped geodes filled with SiO₂ group minerals (agates, amethyst, etc.). Similar basaltic bodies are found in other part of the High Atlas Mts. The most common are in the vicinity of Agouim, where they build a mountain range parallel to the main Atlas range or occur along the road to Ouarzazate. Their thickness is up to few hundred meters, and their length is more than 70 km. Agates occur in practically all the basaltic suites in the area and few names are used to

describe the localities (Agouim-Al Hama, Tizi-n-Tichka, and Agouim-Sour). Our studied samples were collected in the basaltoids mountain range on the left side of the road connecting Agouim and Lake Ifni close to village Sour. Basaltic rocks outcrop are smaller in the Asni area, where they cover the area up to a few km long and are about 300 m thick. Generally, at least four different basaltic suites seem to be recognized in the High Atlas Mts. One of the most interesting regions for agates is the Agouim–Tizi-n-Tichka area, where agates are found at many places together with carnelian, jasper, and quartz crystals.

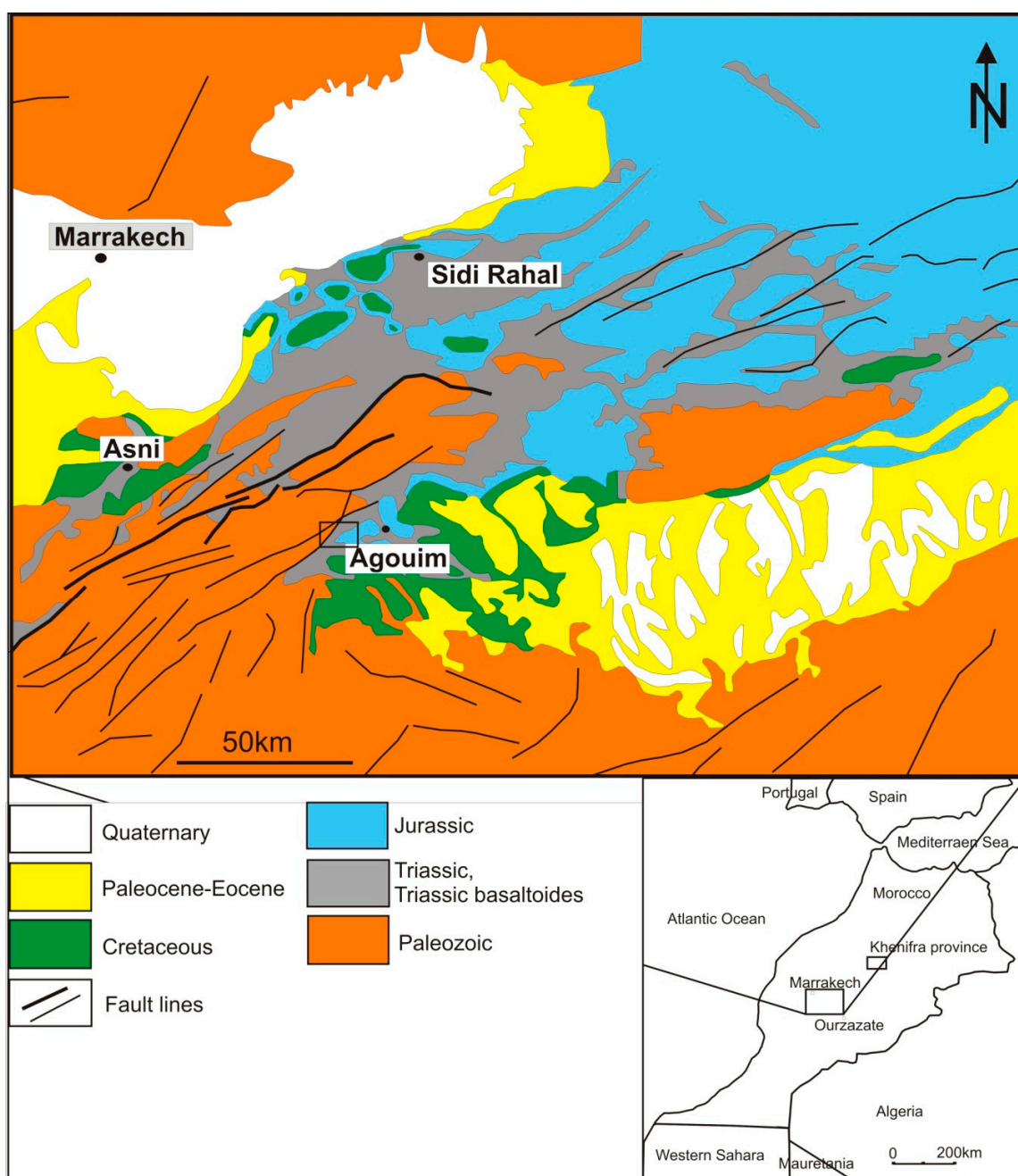


Figure 1. Simplified geological map of the Western Atlas area focusing on the studied agate occurrences (rectangles mark areas of study in Agouim and well as Kerrouchen in Khenifra).

The agate deposit in the Kerrouchen–Ahouli area was found at the beginning of this century [15]. That area is situated in the Khénifra province (Central Morocco), and borders the Middle Atlas on the south, Rif Mountains on the north, and Wadi Muluja on the east. Agate samples are collected there in

the Triassic or lower Jurassic basaltoids or their weathered cover. The outcrops of the basaltic rocks cover an area more than 10×20 km in Kerrouchen and a much larger area in Ahouli.

3. Material and Methods

The samples of Moroccan agates from Asni and Agouim were examined using the Motic SNZ-168 stereoscopic microscope with 7.5–50 \times magnification (Xiamen, China) coupled with a digital camera. The preliminary quality assessment of the material was made, and specific objects were selected for further investigations.

The selected samples were observed in transmitted light using a polarizing microscope (Olympus BX 51 and BA310POL, with a magnification range from 40 \times to 400 \times) (Olympus Corporation, Shinjuku Monolith, Tokyo, Japan). The identification of ore minerals under reflected light was made using a polarizing microscope Nikon Eclipse. The microscope was coupled with a DP 12 camera used for photographic documentation.

The backscattered electron observations were performed on polished sections using a FEI Quanta 200 electron microscope equipped with energy-dispersive spectroscopy (FEI Company, Fremont, CA, USA). The system was operated in low-vacuum mode, at 20 kV accelerating voltage and 50 μ A current. The working distance was 10 mm. The semi-quantitative analysis of target elements were supported by ZAF correction (Z- atomic number correction, A- absorption correction, F- fluorescence absorption).

The Raman spectra of silica phases and abundant solid inclusions were recorded using a Thermo Scientific DXR Raman microscope (Thermo Scientific, Waltham, MA, USA), equipped with 100–10 \times magnification objectives, operating in a confocal mode and working in the backscatter geometry. The polished sample pieces were excited with a 532 nm high-power laser. The laser focus diameter was 1–2 μ m. The Raman spectra of bituminous matter and Fe compounds were acquired using lower laser power (1–2 mW) in order to avoid heating effects. The spectra were corrected for background by the sextic polynomial method using Omnic software attached to the Thermo Scientific DXR Raman microscope. The identification of mineral phases was supported by CrystalSleuth software (ruff project).

4. Results

4.1. Field and Macroscopic Observations

The agates from Asni and Agouim usually form small specimens, ranging in size from 2–3 cm to a maximum of 15 cm in diameter (Figure 2). During field work, it was possible to find specimens up to 50 cm in size, but they are very rare in these regions. Most of the agates are of lithophile-type rarely occur as vein types. In general, they exhibit monocentric or polycentric banding, with alternate white and grey zones varying in sizes of the individual layers. Other types, rich in red and brown incrustation are quite rare and reach a maximum of 10% of all agates found in these localities. These specimens are mainly found in Asni, where agates were collected in the vicinity of hematite veins crosscutting basaltic rocks.

Agates from Asni are mainly of the vein type (Figure 2A,B). Each has a different shape, size, color, and pattern. As for dominant color, they seem to be similar to Sidi Rahal agates [24]. The agate nodules from Asni are mainly grey-white or red-grey with a characteristic red-orange or pink external rim. In the crustal part of an agate's geode, white-grey chalcedony coexists with colorless quartz. When cut and polished, they reveal various landscape and pseudostalactitic patterns. However, the majority of them are monocentric, with an aperture left in the center or filled with the youngest generation of silica polymorph.

Agates of Agouim, like those from Kerrouchen area [25], are characterized by a wealth of morphological types and structural/textural diversity. They mainly represent monocentric spherical or oval agates, with an aperture filled with idiomorphic rose-orange quartz crystals, or with a central zone stratified horizontally (Figure 2C–F). Many polycentric agates have irregular shapes and the silica

matrix alongside coloring oxides, create patterns sometimes similar to stalactite or pseudostalactite, in shades of grey, orange, pink, and red. It is also not uncommon for agates of the vein-type to have reddish-brown colors, which predominate at the outer zones, while lighter, greyish-blue colors dominate in the inner zones, giving an impression of brittle filling.

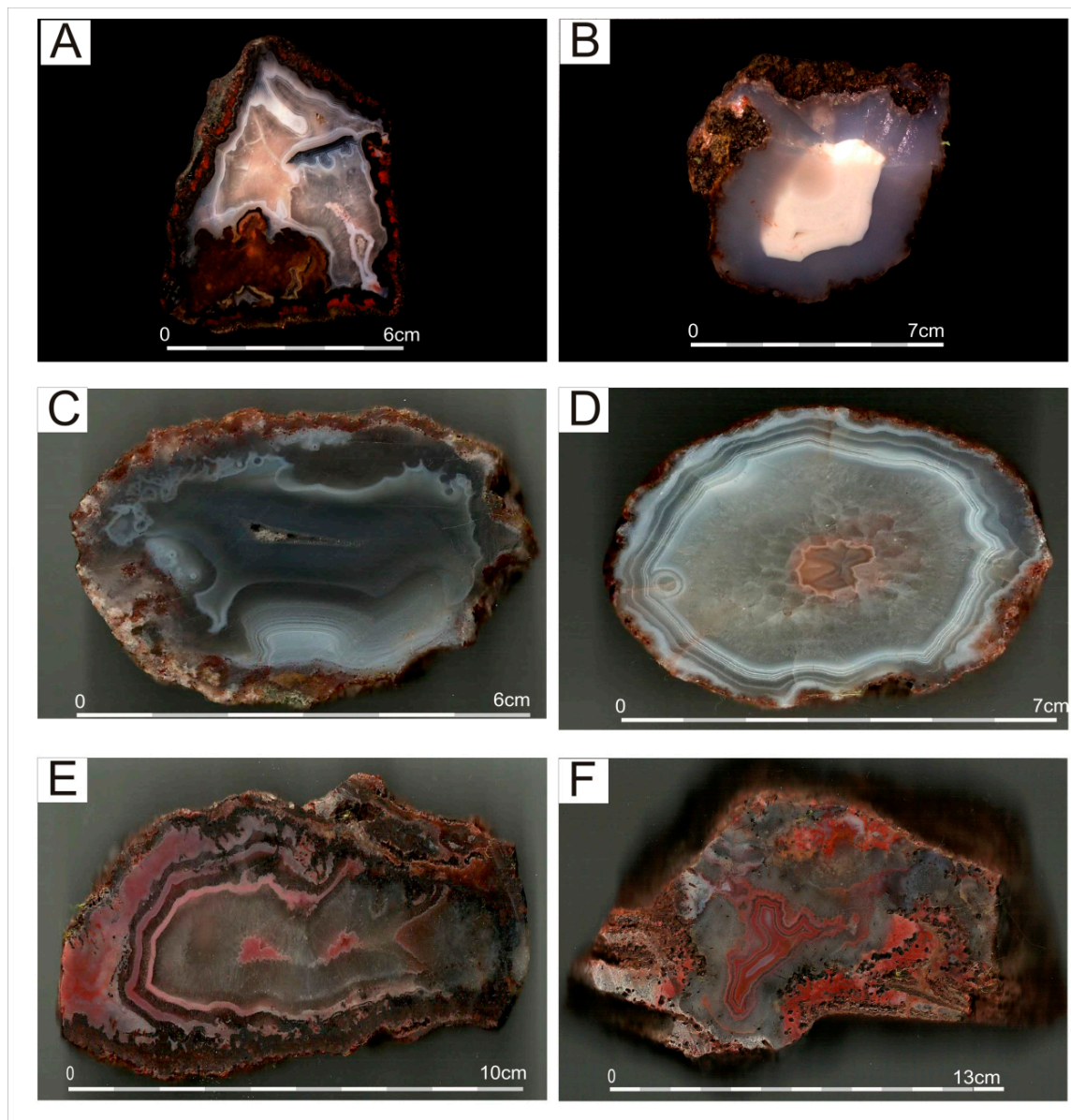


Figure 2. Macrophotographs of examined Moroccan agates: (A,B) Agates from Asni showing either polycentric (A) or monocentric fabrics (B). Note the presence of black and red-colored pigments distributed along the external margin of the geode made of polycentric agate. (C,D) Monocentric agates from Aguaim marked by wall-lining arrangement of alternating dark and light-colored chalcedonic bands (C). Note the occurrence of a well-developed quartz-rich center (D), as well as abundant hematite pigments distributed along particular chalcedonic layers (E,F).

4.2. Microscopic Characteristics in Transmitted and Reflected Light

The silica matrix of agates from Asni and Aguaim do not present remarkable differences in terms of microtextural features and an abundance of SiO_2 -rich phases. Agates from both localities consist predominantly of various cryptocrystalline silica polymorphs including alternating length-fast (normal chalcedony with c-axis situated perpendicular to the fibers) and length-slow/quartzine (c-axis parallel

to the fibers) chalcedony, as well as zebraic chalcedony (length-fast with a helical twisting of fibers along c-axis). These silica phases occur in the form of rounded, bundle-like or polygonal-shaped spherulites, but also appear as fibrous radial aggregates radiating towards the center of the geode (Figure 3A–C). Chalcedonic spherules (especially zebraic chalcedony) are sometimes associated with so-called jigsaw puzzle (mosaic) quartz characterized by sinusoidal, or interpenetrating grain boundaries (Figure 3C) [29,30]. Some of the agates host prismatic quartz crystals, occupying the internal part of the nodule and amounting up to 1 mm in size. Under crossed polarizers, these crystals locally reveal divergent extinction characteristics resulting in a feathery (splitery) or flamboyant appearance, developed both within the single crystals and on the margins of prismatic crystals with a euhedral core (Figure 3D) [30]. Additionally, subparallel wall-lining quartz crystals are locally marked by the presence of μm -sized growth lines, so-called Bambauer quartz [31] (Figure 3E). The growth lines are also frequently impregnated by red, minute hematite pigment. The outer parts of agate nodules comprise tabular and elongated molds filled either with microcrystalline silica associated with intergrowths of calcite and/or barite (Figure 3F,G). Such an alignment of silica phases slightly resembles pseudo-bladed microtexture reported by Dong and colleagues [30] and Moncada and co-workers [32].

Agate nodules are accompanied by secondary hydrothermal phases including celadonite, Fe-oxides/hydroxides, and calcite. Celadonite forms green or bluish-green dull clay masses as well as minute scales (Figure 3H). Fe oxides/hydroxides occur in two generations. The first one is characterized by irregular and ragged crystals randomly distributed within the silica matrix. The second one is found in the outer parts of the nodules and comprises needle-like or capillaceous crystals located perpendicular to chalcedonic-quartz bands (Figure 3H). Conversely, calcite occurs mostly as rhombohedral crystals up to 2 mm in size, but some crystals seem to be overprinted by microcrystalline silica phases (Figure 3G).

In reflected light, numerous kidney shaped aggregates of goethite, clearly “rooted” in the host rock, as well as spectacular, large rosette forms of idiomorphic goethite crystals and/or lepidocrocite (higher reflectivity), were found in the silica matrix of agates. The numerous goethite pseudomorphs after quartz/barite crystals were also observed. They were surrounded by lepidocrocite-forming characteristic halo effects around the goethite pseudomorphs (Figure 4A). In agates from Asni and Agouim, the inclusions of pyrite (Figure 4B,C), as well as Cu-bearing phases like bornite, chalcocopyrite, and covellite were also found. Moreover, the presence of pseudomorphs filled by barite and hematite was noted (Figure 4D). All these inclusions are often accompanied by small grains of titanium oxides (rutile, anatase) and by various types of organic matter, whose presence is confirmed by the effects of fluorescent glow visible under the UV lamp.

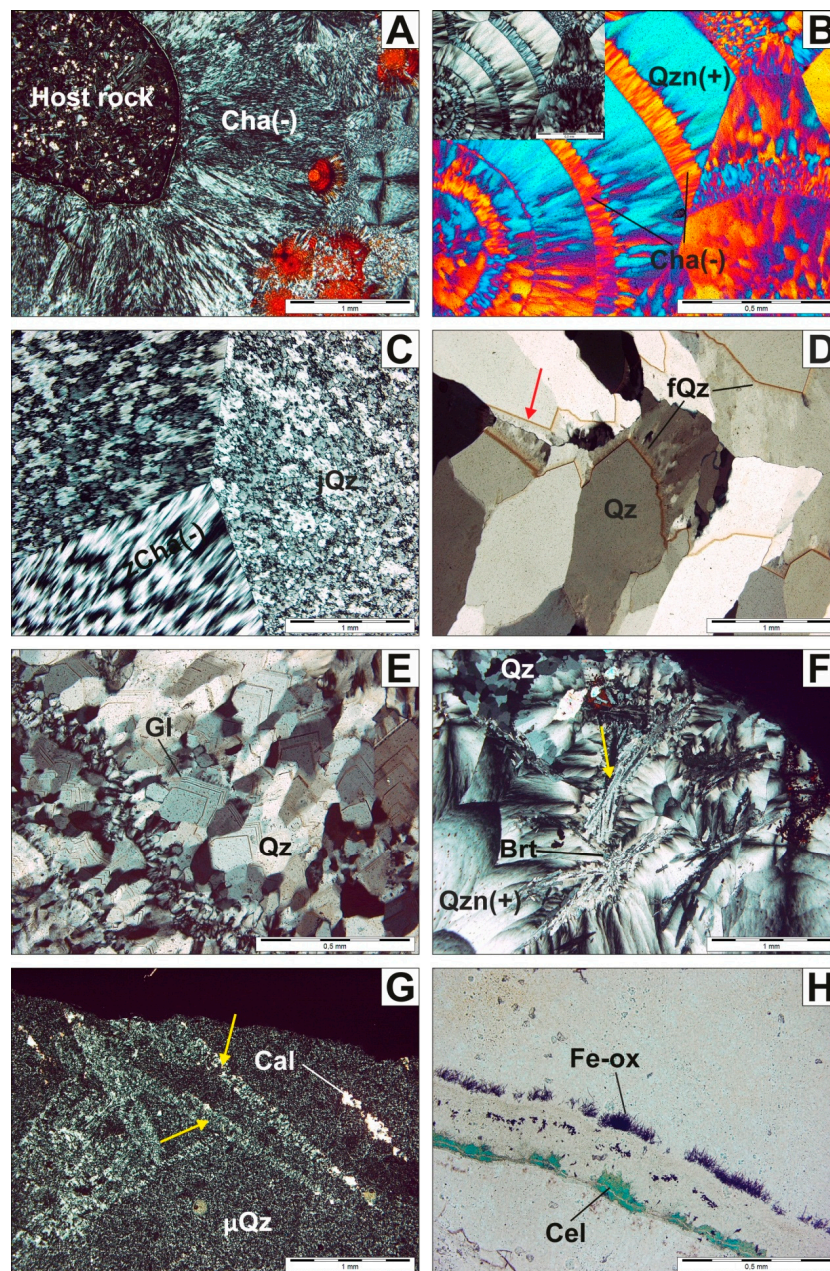


Figure 3. Photomicrographs of agate samples. (A) Bundle-like accumulation of chalcedonic spherules and Fe-oxides at the contact with host rocks comprising tabular plagioclases and anhedral pyroxenes—PX. (B) Length-fast chalcedony interlayered with length-slow chalcedony (quartzine)—NX with a gypsum plate inserted from the lower left. (C) Polygonal-shaped crystals of zebraic chalcedony; note the vanishing chalcedony fibrous texture at the expense of jigsaw puzzle quartz (with interpenetrating grain boundaries)—PX. (D) Internal part of the geode occupied by euhedral prismatic quartz crystals with feathery/spilintery appearance; red arrow points to the minute pigment of oxides developed at the edges of quartz crystals—PX. (E) Discrete growth lines (so-called Bambauer quartz) developed within quartz crystals. (F,G) Plate-like form of silica phases associated with minor barite (almost indistinguishable from quartz due to low birefringence) and calcite. (H) Celadonite accompanied by needle-like crystals of Fe-oxides in the external areas of the agate. Abbreviations: Cha(-): length-fast chalcedony; Qzn(+): length-slow chalcedony (quartzine); zCh(-): zebraic chalcedony; fQz: feathery quartz (with undulose extinction); Gl: growth lines; jQz: mosaic quartz (with interpenetrating grain boundaries); Qz: megaquartz (>20 μm in size); μQz : microcrystalline quartz (<20 μm in size); Cel: celadonite; Cal: calcite; Fe-ox: iron oxides/hydroxides.

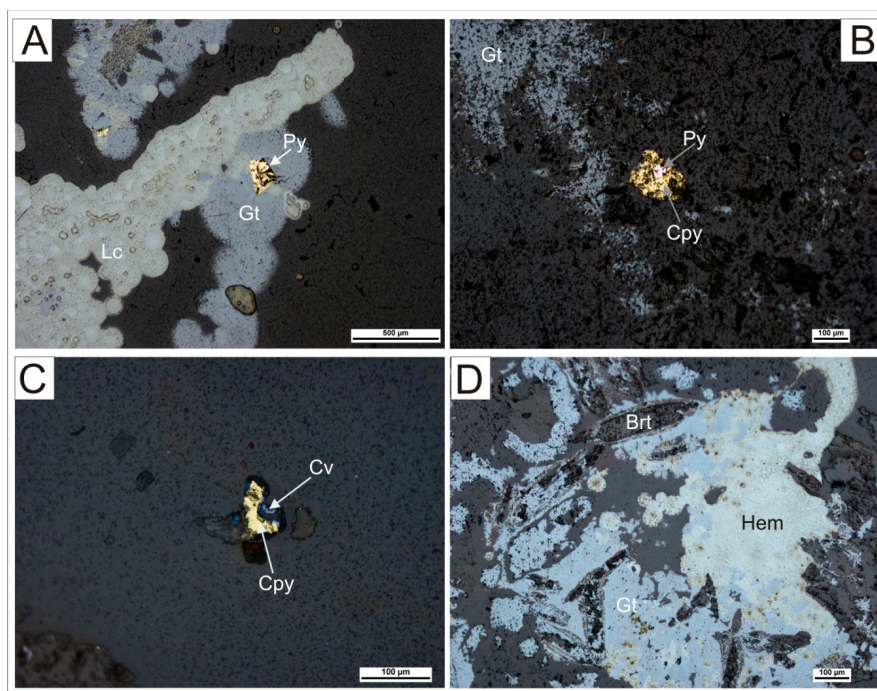


Figure 4. Images in reflected light: (A) kidney-shaped clusters of goethite (Gt) and lepidocrocite (Lc) and single pyrite grains (Py); (B) pyrite (Py) with chalcopyrite intergrowths in association with goethite; (C) chalcopyrite (Cpy) replaced by covellite (Cv); (D) large pseudomorphosis after barite filled by hematite (Hem) and goethite (Gt) with remnants of barite (Brt).

4.3. Scanning Electron Microscopy (SEM)

Under SEM observations agates show microporosity of the silica matrix and some fissures were identified. The most micropores and micro-fissures are empty, only locally filled with quartz or carbonates (calcite), forming tiny and well-shaped crystals. Within the silica matrix abundant solid inclusions were identified. Fe compounds occur as thin needles, spherical and irregular forms, which are the most abundant inclusions in Moroccan agates. The vast majority of mineral inclusions are also represented by calcite, which forms individual crystals or compact aggregates. Celadonite and chlorite occur in the outer part of agates, near the host rock. They form fibrous crystals filling the nests within the silica matrix. Barite inclusions were identified only in agates from Agouim. The copper sulfides (i.e., bornite, covellite, and chalcopyrite), as well as sylvite, form small clusters embedded within the silica matrix (Figure 5A,B).

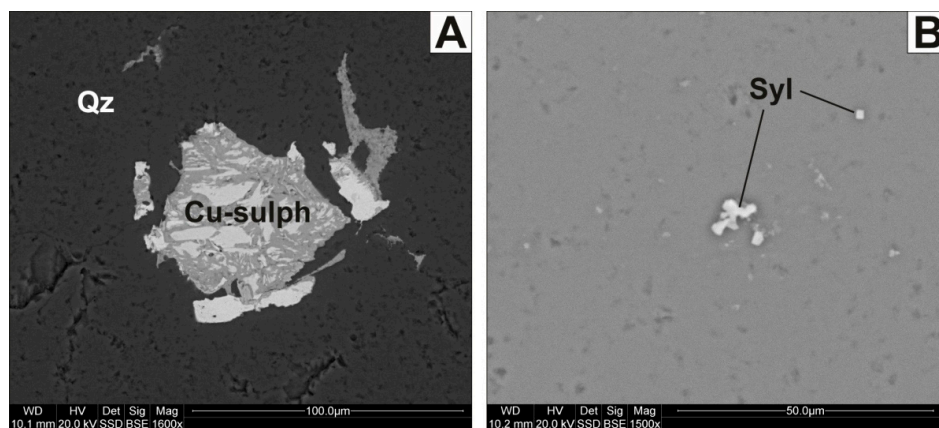


Figure 5. Back Scattered Electrons (BSE) picture of the inclusions in agates from Agouim area (A) Cu-compounds (Cu-sulph) in agate matrix. (B) Small inclusions of sylvite (Syl) in agate matrix.

4.4. Raman Micro-Spectroscopy (RS)

Raman micro-spectroscopy analyses showed that agates from Asni and Agouim were mainly built of low quartz with diagnostic bands at 463, 357, 210, and 130 cm^{-1} , as well as subordinate moganite with a marker band at 502 cm^{-1} (Table 1) [7]. For a quantitative evaluation of the moganite content in the studied samples, the method proposed by Götze et al. [7] using the relations between intensity of moganite and α -quartz peaks (502 and 463 cm^{-1}) was applied. The estimated local moganite content ranges from 0% to 56%, and 0% to 78% for Asni and Agouim agates, respectively (Table 2).

Table 1. Example of the Raman spectra for all identified minerals.

Raman Bands (cm^{-1})	Solid Phase	References
463 (s), 357 (w), 210 (m), 130 (m)	low quartz	[7]
502 (s)	moganite	[7]
1323 (s), 669 (w), 613 (m), 497 (w), 413 (s), 293 (s), 248 (m), 226 (s)	hematite	[33,34]
1316 (m), 685 (m), 553 (m), 388 (s), 301 (m), 247 (w)	goethite	[33]
610 (s), 443 (s)	rutile	[35]
708–688 (s), 569 (w)	magnesiochromite	[36]
1595 (s), 1362 (s)	bituminous matter	[37,38]
3559 (m), 3534 (m), 1620 (m), 1116 (w), 1075 (w), 959 (m), 700 (s), 547 (s), 456 (m), 399 (w), 382 (w), 277 (m)	celadonite	[39]
1088 (s), 714 (w), 285 (m), 158 (m)	calcite	[40,41]
1142 (w), 989 (s), 649 (w), 619 (w), 465 (m), 456 (w)	barite	[42,43]

Note: s, m, and w refer to strong, medium, and weak intensity bands, respectively.

Table 2. Local moganite content and integral ratio of 502 cm^{-1} and 463 cm^{-1} Raman bands in agate samples from Asni and Agouim.

Analytical Material	Raman Band Integral Ratio $I_{(502)}/I_{(463)}$			Local Moganite Content		
	(%)	Mean (%)	Standard Deviation	(wt.%)	Mean (%)	Standard Deviation
Asni (11)	0.0–23.2	13.7	7.2	0.0–56.0	38.3	17.4
Agouim (34)	0.0–65.2	9.1	11.8	0.0–78.0	25.5	18.5

Note: the number of analytical spots are in the parentheses.

Apart from silica phases, agates host abundant mineral and organic inclusions. Goethite and hematite were recognized as major Fe-bearing compounds. Hematite forms characteristic red colored spherical or irregularly-shaped aggregates. Its presence is proved by its Raman bands at 1323, 669, 613, 497, 413, 293, 248, and 226 cm^{-1} . The bands at 613, 413, 293, and 248 cm^{-1} are due to Fe–O symmetric bending vibrations, while the bands at 669, 497, and 226 cm^{-1} originate from Fe–O symmetric stretching vibrations (Table 1) [33,34]. The most intensive band at ca. 1323 cm^{-1} , attributed to the second-order 2LO mode with 2Eu symmetry due to defects in its lattice, is diagnostic for disordered hematite [44]. Goethite forms orange-colored aggregates irregularly scattered within the agate matrix. It is evidenced by marker bands at 1316, 685, 553, 388, 301, and 247 cm^{-1} . The most intensive band at 388 cm^{-1} is assigned to Fe–O–Fe/OH symmetric stretching vibrations [33]. The other bands at 685 and 553 cm^{-1} area assigned to Fe–O symmetric stretching and Fe–OH asymmetric stretching vibrations, respectively. The intensive line at 301 cm^{-1} corresponds to Fe–OH symmetric bending vibrations [33]. The broad 2LO band at 1316 cm^{-1} is characteristic of various Fe-oxide and Fe-hydroxide with disordered structures [44].

Raman spectra recorded for dark brown and black inclusions hosted in agates revealed the presence of two broad bands found in the regions of 708–688 cm^{-1} and ca. 569 cm^{-1} , which seemed to be diagnostic of spinel group mineral (i.e., magnesiochromite [36]) (Table 1). The most intensive

band at ca. 708–688 cm^{-1} was attributed to $\nu_1(A_{1g})$ symmetric stretching vibrations of the BO_6 groups (where B = Cr, Al, Fe), whereas the weak band at 569 cm^{-1} was due to $\nu_3(F_{2g})$ mode [36].

Rutile manifested its presence by two major bands found at 610 and 443 cm^{-1} , which were assigned to A_{1g} and E_g modes, respectively [35].

Local mineral inclusions are accompanied by bituminous matter, whose presence is proved by its two (first-order) marker bands at 1595 and 1362 cm^{-1} (Figure 6, Table 1) [37,38]. Based on the shape of the Raman spectrum recorded for bituminous matter, it was found, that the most intensive and broad band at 1595 cm^{-1} in the case of low temperature samples is assigned to the disordered D2 band, whereas the band at 1362 cm^{-1} is called a disordered carbon band (D1) [45]. The relative intensities of these two bands, their width and the height of the saddle suggest that bituminous matter represents low-grade carbonaceous material with features typical of amorphous carbon [45,46].

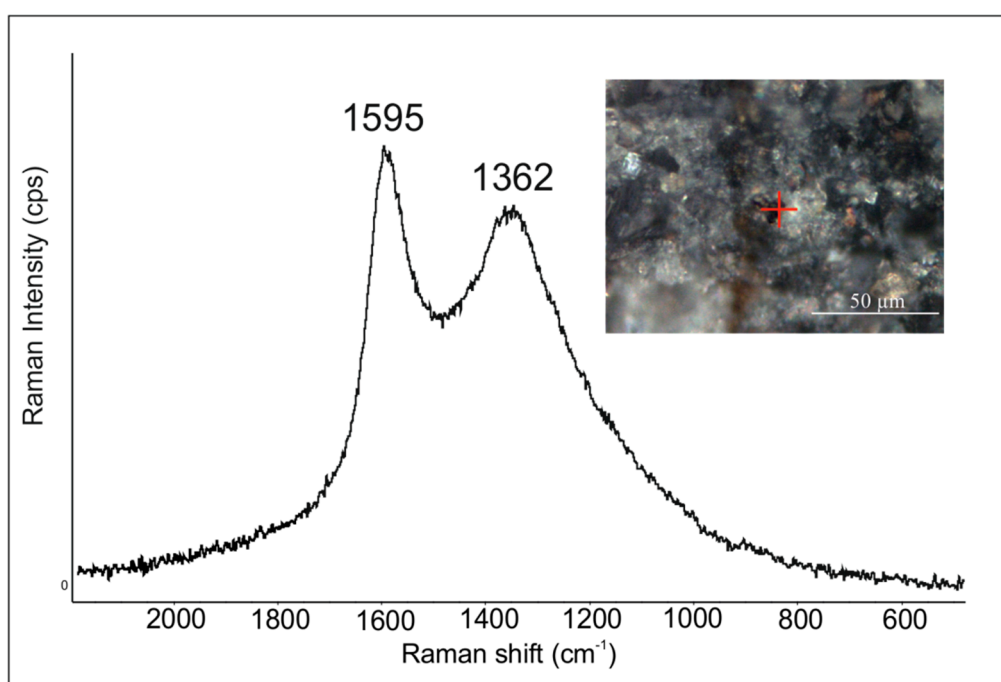


Figure 6. Microphotograph and Raman spectrum of low-grade carbonaceous material in the range of 2200–500 cm^{-1} . Analytical spot was marked by red cross.

At the outermost parts of agate nodules, green colored and irregularly-shaped aggregates are frequently found. The Raman spectrum recorded for these inclusions revealed the presence of numerous bands found at 3559, 3534, 1620, 1116, 1075, 959, 700, 547, 456, 399, 382, and 277 cm^{-1} , diagnostic of celadonite (Figure 7, Table 1) [39]. In the spectral region of 300–800 cm^{-1} the band is mainly due to Si–O–R and R–O-bending vibrations (where R is an octahedral cation). The bands at 1116, 1075, and 959 cm^{-1} are assigned to in-plane Si–O stretching vibrations [39]. The two narrow bands at 2559 and 3534 cm^{-1} and one broad band ca. 1620 cm^{-1} are due to hydroxyl stretching and bending vibrations, respectively [39].

Moreover, agates from Agouim contain inclusions of carbonates and sulfides. The presence of calcite is evidenced by its marker bands at 1088, 714, 285, and 158 cm^{-1} . The most intense ν_1 band at 1088 cm^{-1} corresponds to the symmetric stretching vibrations of CO_3 group (Table 1). The Raman ν_4 line at 714 cm^{-1} is due to asymmetric bending vibrations [cf. 40]. The lower wavenumber region of calcite at 285 and 158 cm^{-1} reflects lattice modes [41].

Barite forms tabular crystals randomly distributed in agate matrix. It is clearly marked by bands at 1142, 989, 649, 619, 465, and 456 cm^{-1} (Table 1). The dominant ν_1 band of barite was found at 989 cm^{-1} and arose from the symmetric stretching of SO_4 . The ν_2 bands at ca. 465–456 cm^{-1} and ν_4 band at ca. 649–619 cm^{-1} were assigned to in-plane and out-of-plane bending vibrations, respectively [42,43].

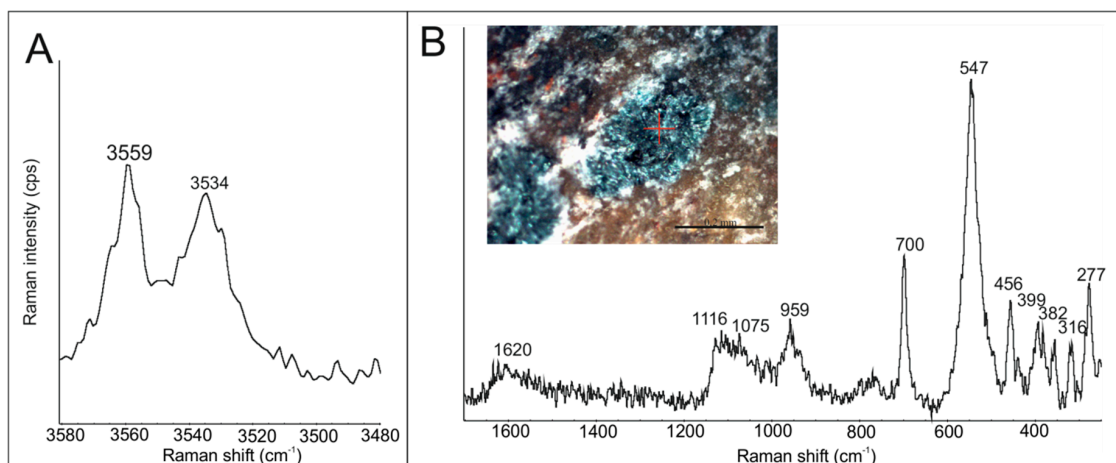


Figure 7. Microphotograph and Raman spectra of celadonite in the range of 3580–3480 cm^{-1} (A) and 1700–250 cm^{-1} (B). Analytical spot was marked by red cross.

5. Discussion

Agates from Agouim and Asni in Western Atlas Mountains are mainly built of length-fast and length-slow chalcedony with local admixture of moganite (from 0% up to 78%). The moganite contents in agates, estimated with Raman micro-spectroscopy, seem to be too high for agates hosted in Triassic rocks [8,47]. The significantly overestimated mean values of moganite result from the Raman measurements in individual points, where moganite locally predominates over low quartz. According to Götze and colleagues [7], determination of moganite content using Raman spectroscopy may be overestimated as compared with the results provided by X-ray powder diffraction. These variations may be due to the presence of moganite nanocrystals or moganite nano-range lamellae that are not large enough to contribute to the Bragg reflection, but may simultaneously induce the effect of Raman scattering [7,48]. The occurrence of alternating crystals of length-fast and length-slow chalcedony gives a clue for remarkable fluctuations of physicochemical conditions during agates formation. The former silica polymorph is indicative of neutral to acidic and/or sulphate-poor environments, whereas the latter is believed to be associated with alkaline/sulfur-rich solutions [49]. However, it should be noted that the above discrimination was later undermined by Keene [50]. The abundance of growth lines (so-called Bambauer quartz) also invokes rapid changes in pH and/or silica content in low-temperature parental fluids [10,51], that were necessary for agate formation. Additionally, the abundance of so-called, pseudobladed silica could be explained by metasomatic replacement of pre-existing plate-like barite and/or calcite by microcrystalline quartz [30,32]. The development of this fabric could be induced by boiling-related conditions [32], referring to the rapid drop of temperature and pressure that result in the formation of coexisting fluid-rich and vapor-rich phases. The presence of boiling could be further responsible for the formation of ore-related phases, such as Fe and Cu sulfides found within the silica matrix of agates. The feathery and jigsaw puzzle quartz microtextures found within agate nodules provide, in turn, strong evidence for the recrystallization of pre-existing massive chalcedony or amorphous silica [52–54].

The abundance of hematite points to the high activity of iron in silica bearing medium. Furthermore, needle-like arrangement of Fe-oxides (Figure 3F) along chalcedonic bands originated from self-purification processes, whereas irregular or oval-shaped crystals of these phases possibly represent primary impurities [2]. The presence of celadonite, found in the outer parts of agate nodules, reflects oxidizing near-surface conditions and argues for the influence of slowly-circulating K- and Mg-rich solutions during the initial stage of agate formation [55,56]. The origin of poorly ordered and low-grade solid carbonaceous matter, forming irregular accumulations within the silica matrix of agates, is probably connected with the low-hydrothermal activity of SiO_2 -bearing fluids (i.e., meteoric waters). Kříbek et al. [57] noted that precipitation of hydrothermal carbonaceous matter occurred due

to the supersaturation of C–O–H fluids (containing CH₄ or CO₂) with carbon at the deeper or middle crustal levels.

6. Conclusions

The agates from Agouim and Asni display exceptionally high diversity in microtextural features as well as accessory compounds, forming solid inclusions. They exhibit a wealth of colors, morphological features, and patterns. They are similar to agates occurring in other Moroccan localities, such as Sidi Rahal and Kerrouchen-Ahouli. All gems contain assemblages of similar solid inclusions, which are mainly represented by hematite, goethite, rutile, as well as barite, copper sulfides, and carbonates, which were probably formed during the post-magmatic processes of the hydrothermal stage and/or the tectonic processes which affected the area of High Atlas during the Alpine orogen system. Asni and Agouim are located close to the main Atlas mountain ridge as well as to the main tectonic lines, so the hydrothermal solution had a greater opportunity to alter agates in that area, compared to Kerrouchen or Sidi Rahal regions, which are located outside the main tectonic zones [18,22,23].

Agates from the Atlas Mts. are hosted by the same type of volcanic rocks (basalt), which were assembled during the Triassic period [24,25]. The main feature, which distinguishes agates from Sidi Rahal compared to agates from the other localities, is the presence of opal CT (disordered α - cristobalite, α -tridymite) which was not confirmed in agates from Agouim-Asni-Kerrouchen areas. The existence of opal CT in agates from Sidi Rahal could be attributed to the transformation of amorphous silica deposited within basaltic rocks during the initial stage of agate formation following the reaction: opal A \rightarrow opal CT \rightarrow opal C \rightarrow chalcedony [58]. Hence, it is assumed that agates from Sidi Rahal exhibiting the presence of remnants of primary silica, that are not fully recrystallized into chalcedony, could be the younger than gems from other regions of Morocco. However, the presence of quite elevated moganite content (av. 25–38 wt.%, Table 2) in the agates from the study area infers that their formation was closely related to the syn- and post-volcanic alterations of the host rocks. According to Moxon and Ríos [8], moganite tends to recrystallize into more stable and water-poor α -quartz after silica deposition within particular cavities. Hence, this silica polymorph is nearly absent in agates found within relatively old volcanos (i.e., of Early-Permian age; see [59]), but could still be present in relatively young host basaltoids, such as those found in the vicinity of Asni and Agouim, but also Sidi Rahal and Kerrouchen.

Author Contributions: Field work, as well as manuscript writing by J.P.; microscopic study by D.S. and D.Z.; EDS study and writing by L.N.-N.; figure editing, review and manuscript editing by T.P.; Raman spectroscopy by M.D.-S. and T.T. All authors have read and agreed to the published version of the manuscript.

Funding: This work was supported by research grant no 16.16.140.315 from the AGH University of Science and Technology.

Acknowledgments: The mineral collectors, Jacek Szczerba, Mariusz Jarzyński, and Andrzej Kuźma are greatly acknowledged for providing Moroccan agate samples for the study. We would like to thank the anonymous reviewers as well as handling editor Luke Wu for their useful and friendly comments which helped to improve the manuscript.

Conflicts of Interest: The authors declare no conflicts of interest.

References

1. Götze, J.; Plötze, M.; Tichomirowa, M.; Fuchs, H.; Pilot, J. Aluminum in quartz as an indicator of the temperature of formation of agate. *Mineral. Mag.* **2001**, *65*, 407–413. [[CrossRef](#)]
2. Götze, J.; Möckel, R.; Kempe, U.; Kapitonov, I.; Vennemann, T. Characteristics and origin of agates in sedimentary rocks from the Dryhead area, Montana, USA. *Mineral. Mag.* **2009**, *73*, 673–690. [[CrossRef](#)]
3. Götze, J. *Agate-Fascination between Legend and Science*; Agates Zenz, J., III, Ed.; Bode-Verlag: Salzhemmendorf, Germany, 2011; pp. 19–133.
4. Moxon, T.; Nelson, D.R.; Zhang, M. Agate recrystallization: Evidence from samples found in Archaean and Proterozoic host rocks, Western Australia. *Aust. J. Earth Sci.* **2006**, *53*, 235–248. [[CrossRef](#)]

5. Heaney, P.J. A proposed mechanism for the growth of chalcedony. *Contrib. Mineral. Petrol.* **1993**, *115*, 66–74. [[CrossRef](#)]
6. Graetsch, H. Structural characteristics of opaline and microcrystalline silica minerals. *Rev. Mineral. Geochem.* **1994**, *29*, 209–232.
7. Götze, J.; Nasdala, L.; Kleeberg, R.; Wenzel, M. Occurrence and distribution of “moganite” in agate/chalcedony: A combined micro-Raman, Rietveld, and cathodoluminescence study. *Contrib. Mineral. Petrol.* **1998**, *133*, 96–105. [[CrossRef](#)]
8. Moxon, T.; Ríos, S. Moganite and water content as a function of age in agate: An XRD and thermogravimetric study. *Eur. J. Mineral.* **2004**, *16*, 269–278. [[CrossRef](#)]
9. Götze, J.; Nasdala, L.; Kempe, U.; Libowitzky, E.; Rericha, A.; Vennemann, T. The origin of black colouration in onyx agate from Mali. *Miner. Mag.* **2012**, *76*, 115–127. [[CrossRef](#)]
10. Richter, S.; Götze, J.; Niemeyer, H.; Möckel, R. Mineralogical investigations of agates from Cordón de Lila, Chile. *Andean Geol.* **2015**, *42*, 386–396.
11. French, M.W.; Worden, R.H.; Lee, D.R. Electron backscatter diffraction investigation of length-fast chalcedony in agate: Implications for agate genesis and growth mechanisms. *Geofluids* **2013**, *13*, 32–44. [[CrossRef](#)]
12. Sobczak, N.; Sobczak, T. *Big Encyclopedia of Gemstones*; Polskie Wydawnictwa Naukowe Publishing House: Warsaw, Poland, 1998; p. 422. (In Polish)
13. Manecki, A. *Agates and Silicites: Genesis of Beauty—a Beauty of Genesis*; AGH—The University of Science and Technology Publishing House: Krakow, Poland, 2015; p. 90. (In Polish)
14. Żaba, J. *Illustrated Dictionary of Rocks and Minerals*; Videograf, II: Katowice, Poland, 2003; p. 503. (In Polish)
15. Jahn, S.; Bode, R.; Lyckberg, P.; Medenbach, O.; Lierl, H.-J. *Marokko. Land der Schönen Mineralien und Fossilien*; Bode-Verlag GmbH: Salzhemmendorf, Germany, 2003; p. 535. (In German)
16. Zenz, J. *Achate*; Bode-Verlag GmbH: Salzhemmendorf, Germany, 2005; p. 656. (In German)
17. Zenz, J. *Achate-Schätze*; Bode-Verlag GmbH: Salzhemmendorf, Germany, 2009; p. 656. (In German)
18. Bakarar, A. Gold mineralization in the Ourika Gneiss (High Atlas of Marrakech, Morocco): Mineral paragenesis and fluid P-T-X evolution. *Arabian J. Geosci.* **2015**, *8*, 3207–3222. [[CrossRef](#)]
19. Ilmen, S.; Alansari, A.; Bajddi, A.; Ennaciri, A.; Maacha, L. Contribution à l'étude géologique du gisement à Cu, Zn, Pb et Ag-Au d'Amensif (District minier d'Amizmiz, Haut Atlas occidental, Maroc). *Int. J. Innov. Appl. Stud.* **2014**, *6*, 768–783. (In French)
20. Lafforgue, L.; Barbarand, J.; Missenard, Y.; Brigaud, B.; Saint-Bézar, B.; Yans, J.; Dekoninck, A.; Saddiqi, O. Origin of the Bouarfa Manganese Ore Deposit (Eastern High Atlas, Morocco): Insights from Petrography and Geochemistry of the Mineralization. Mineral resources in a sustainable world. In Proceedings of the 13th SGA Biennial Meeting 2015, Nancy, France, 24–27 August 2015; pp. 1949–1952.
21. Rddad, L.; Bouhleb, S. The Bou Dahar Jurassic carbonate-hosted Pb–Zn–Ba deposits (Oriental High Atlas, Morocco): Fluid-inclusion and C–O–S–Pb isotope studies. *Ore Geol. Rev.* **2016**, *72*, 1072–1087. [[CrossRef](#)]
22. Essalhi, M.; Mrani, D.; Essalhi, A.; Toummite, A.; Ali-Ammar, H. Evidence of a high quality barite in Drâa-Tafilalet region, Morocco: A nonupgraded potential. *J. Mater. Environ. Sci.* **2018**, *9*, 1366–1378.
23. Verhaert, M.; Bernard, A.; Saddiqi, O.; Dekoninck, A.; Essalhi, M.; Yans, J. Mineralogy and genesis of the polymetallic and polyphased low grade Fe–Mn–Cu ore of Jbel Rhals deposit (Eastern High Atlas, Morocco). *Minerals* **2018**, *8*, 39. [[CrossRef](#)]
24. Dumańska-Słowik, M.; Natkaniec-Nowak, L.; Weselucha-Birczyńska, A.; Gawel, A.; Lankosz, M.; Wróbel, P. Agates from Sidi Rahal, in the Atlas Mountains of Morocco: Gemological characteristics and proposed origin. *Gems Gemol.* **2013**, *49*, 148–159. [[CrossRef](#)]
25. Natkaniec-Nowak, L.; Dumańska-Słowik, M.; Pršek, J.; Lankosz, M.; Wróbel, P.; Gawel, A.; Kowalczyk, J.; Kocemba, J. Agates from Kerrouchen (the Atlas Mountains, Morocco): Textural Types and Their Gemmological Characteristics. *Minerals* **2016**, *6*, 77. [[CrossRef](#)]
26. Ellero, A.; Ottria, G.; Malusà, M.G.; Ouanaïmi, H. *Structural Geological Analysis of the High Atlas (Morocco): Evidences of a Transpressional Fold-Thrust Belt, Chapter 9 in Sharkov E.; Tectonics-Recent Advances*; InTech: Rijeka, Croatia, 2012; p. 323.
27. Choubert, G.; Marais, J. Geologie du Maroc. In Proceedings of the 19th International Geological Congress, Algiers, Algeria, 8–15 September 1952.
28. Laville, E. Role of the Atlas Mountains (northwest Africa) within the African-Eurasian plate-boundary zone: Comment. *Geology* **2002**, *30*, 1–95. [[CrossRef](#)]

29. Lovering, T.G. *Jasperoid in the United States; its Characteristics, Origin, and Economic Significance* (No. 710); USGS: Reston, VA, USA, 1972; p. 176.
30. Dong, G.; Morrison, G.; Jaireth, S. Quartz textures in epithermal veins, Queensland; classification, origin and implication. *Econ. Geol.* **1995**, *90*, 1841–1856. [[CrossRef](#)]
31. Bambauer, H.U.; Brunner, G.O.; Laves, F. Beobachtungen über Lamellen bau an Bergkristallen. *Z. Krist.* **1961**, *116*, 173–181. (In German) [[CrossRef](#)]
32. Moncada, D.; Mutchler, S.; Nieto, A.; Reynolds, T.J.; Rimstidt, J.D.; Bodnar, R.J. Mineral textures and fluid inclusion petrography of the epithermal Ag–Au deposits at Guanajuato, Mexico: Application to exploration. *J. Geochem. Explor.* **2012**, *114*, 20–35. [[CrossRef](#)]
33. Legodi, M.; de Waal, D. The preparation of magnetite, goethite, hematite and maghemite of pigment quality from mill scale iron waste. *Dyes Pigment.* **2007**, *74*, 161–168. [[CrossRef](#)]
34. Hanesch, M. Raman spectroscopy of iron oxides and (oxy)hydroxides at low laser power and possible applications in environmental magnetic studies. *Geophys. J. Int.* **2009**, *177*, 941–948. [[CrossRef](#)]
35. Balachandran, U.; Eror, N.G. Raman spectrum of titanium dioxide. *J. Solid State Chem.* **1982**, *42*, 276–282. [[CrossRef](#)]
36. Kharbish, S. Raman spectroscopic features of Al-Fe³⁺-poor magnesiochromite and Fe²⁺-Fe³⁺-rich ferrian chromite solid solutions. *Mineral. Petrol.* **2017**, *112*, 245–256. [[CrossRef](#)]
37. Beyssac, O.; Goffe, B.; Petitet, J.-P.; Froigneux, E.; Moreau, M.; Rouzaud, J.-N. On the characterization of disordered and heterogeneous carbonaceous materials by Raman spectroscopy. *Spectrochim. Acta Part A* **2003**, *59*, 2267–2276. [[CrossRef](#)]
38. Starkey, N.A.; Franchi, I.A.; Alexander, C.M.O. A Raman spectroscopic study of organic matter in interplanetary dust particles and meteorites using multiple wavelength laser excitation. *Meteorit. Planet. Sci.* **2013**, *48*, 1800–1822. [[CrossRef](#)]
39. Ospitali, F.; Bersani, D.; Di Lonardo, G.; Lottici, P. ‘Green earths’: Vibrational and elemental characterization of glauconites, celadonites and historical pigments. *J. Raman Spectrosc.* **2008**, *39*, 1066–1073. [[CrossRef](#)]
40. Buzgar, N.; Apopei, A.I. The Raman study of certain carbonates. *Geol. Tomul L* **2009**, *2*, 97–112.
41. Gunasekaran, S.; Anbalagan, G.; Pandi, S. Raman and infrared spectra of carbonates of calcite structure. *J. Raman Spectrosc.* **2006**, *37*, 892–899. [[CrossRef](#)]
42. Dimova, M.; Panczer, G.; Gaft, M. Spectroscopic study of barite from the Kremikovtsi deposit (Bulgaria) with implication for its origin. *Ann. Geol. Penins. Balk.* **2006**, *67*, 101–108. [[CrossRef](#)]
43. White, S.N. Laser Raman spectroscopy as a technique for identification of seafloor hydrothermal and cold seep minerals. *Chem. Geol.* **2009**, *259*, 240–252. [[CrossRef](#)]
44. Marshall, C.P.; Marshall, A.O. Raman Hyperspectral Imaging of Microfossils: Potential Pitfalls. *Astrobiology* **2013**, *13*, 920–931. [[CrossRef](#)] [[PubMed](#)]
45. Kouketsu, Y.; Mizukami, T.; Mori, H.; Endo, S.; Aoya, M.; Hara, H.; Nakamura, D.; Wallis, S. A new approach to develop the Raman carbonaceous material geothermometer for low-grade metamorphism using peak width. *Isl. Arc* **2014**, *23*, 33–50. [[CrossRef](#)]
46. Aoya, M.; Kouketsu, Y.; Endo, S.; Shimizu, H.; Mizukami, T.; Nakamura, D.; Wallis, S. Extending the applicability of the Raman carbonaceous-material geothermometer using data from contact metamorphic rocks. *J. Metamorph. Geol.* **2010**, *28*, 895–914. [[CrossRef](#)]
47. Constantina, C.; Moxon, T. Agates from Gurasada, Southern Apuseni Mountains, Romania: An XRD and Thermogravimetric study. *Carpathian J. Earth Environ. Sci.* **2010**, *5*, 89–99.
48. Zhang, M.; Moxon, T. Infrared absorption spectroscopy of SiO₂-moganite. *Am. Mineral.* **2014**, *99*, 671–680. [[CrossRef](#)]
49. Folk, R.L.; Pittman, J.S. Length-slow chalcedony; a new testament for vanished evaporites. *J. Sediment. Res.* **1971**, *41*, 1045–1058.
50. Keene, J.B. Chalcedonic quartz and occurrence of quartzine (length-slow chalcedony) in pelagic sediments. *Sedimentology* **1983**, *30*, 449–454. [[CrossRef](#)]
51. Rykart, R. *Quarz-Monographie*; Ott Verlag: Thun, Switzerland, 1989; p. 462. (In German)
52. Fournier, R.O. The behavior of silica in hydrothermal solutions. *Rev. Econ. Geol.* **1985**, *2*, 45–60.
53. Saunders, J.A. Silica and gold textures in bonanza ores of the Sleeper Deposit, Humboldt County, Nevada; evidence for colloids and implications for epithermal ore-forming processes. *Econ. Geol.* **1994**, *89*, 628–638. [[CrossRef](#)]

54. Yilmaz, T.I.; Duschl, F.; Di Genova, D. Feathery and network-like filamentous textures as indicators for the re-crystallization of quartz from a metastable silica precursor at the Rusey Fault Zone, Cornwall, UK. *Solid Earth* **2016**, *6*, 1509–1536. [[CrossRef](#)]
55. Odin, G.S.; Desprairies, A.; Fullgar, P.D.; Bellon, H.; Decarreau, A.; Fröhlich, F.; Zelvelder, M. Nature and geological significance of celadonite. In *Green Marine Clays: Oolitic Ironstone Facies, Verdine Facies, Glaukonite Facies and Celadonite-Bearing Rock Facies-A Comparative Study*; Odin, G.S., Ed.; Elsevier: Amsterdam, The Netherlands, 1988; pp. 337–392.
56. Baker, L.L.; Rember, W.C.; Sprenke, K.F.; Strawn, D.G. Celadonite in continental flood basalts of the Columbia River Basalt Group. *Am. Mineral.* **2012**, *97*, 1284–1290. [[CrossRef](#)]
57. Kříbek, B.; Sýkorová, I.; Machovič, V.; Knésl, I.; Laufek, F.; Zachariáš, J. The origin and hydrothermal mobilization of carbonaceous matter associated with Paleoproterozoic orogenic-type gold deposits of West Africa. *Precambrian Res.* **2015**, *270*, 300–317. [[CrossRef](#)]
58. Moxon, T.; Carpenter, M.A. Crystallite growth kinetics in nanocrystalline quartz (agate and chalcedony). *Mineral. Mag.* **2009**, *73*, 551–568. [[CrossRef](#)]
59. Powolny, T.; Dumańska-Słowik, M.; Sikorska-Jaworowska, M.; Wójcik-Bania, M. Agate mineralization in spilitized Permian volcanics from “Borówno” quarry (Lower Silesia, Poland) –microtextural, mineralogical, and geochemical constraints. *Ore Geol. Rev.* **2019**, *114*, 103–130. [[CrossRef](#)]



© 2020 by the authors. Licensee MDPI, Basel, Switzerland. This article is an open access article distributed under the terms and conditions of the Creative Commons Attribution (CC BY) license (<http://creativecommons.org/licenses/by/4.0/>).